Integration of High-Tc Superconductors with High-Q-Factor Oxide Mechanical Resonators

ADVANCED FUNCTIONAL MATERIALS
www.afm-journal.de

Integration of High-Tc Superconductors with High-Q-Factor Oxide Mechanical Resonators

Nicola Manca, Alexei Kalaboukhov, Alejandro E. Plaza, Leonélio Cichetto Jr., Eric Wahlberg, Emilio Bellingeri, Francesco Bisio, Floriana Lombardi, Daniele Marré, and Luca Pellegrino*

Micro-mechanical resonators are building blocks of a variety of applications in basic science and consumer electronics. This device technology is mainly based on well-established and reproducible silicon-based fabrication processes with outstanding performances in term of mechanical *Q*-factor and sensitivity to external perturbations. Broadening the functionalities of micro-electro-mechanical systems (MEMS) by the integration of functional materials is a key step for both applied and fundamental science. However, combining functional materials with silicon-based devices is challenging. An alternative approach is directly fabricating MEMS based on compounds inherently showing non-trivial functional properties, such as transition metal oxides. Here, a full-oxide approach is reported, where a high-T_c superconductor $YBa_2Cu_3O_7$ (YBCO) is integrated with high *Q*-factor micro-bridge resonators made of single-crystal $LaAlO_3$ (LAO) thin films. LAO resonators are tensile strained, with a stress of about 350 MPa, show a *Q*-factor above 200k, and have low roughness. YBCO overlayers are grown ex situ by pulsed laser deposition and YBCO/LAO bridges show zero resistance below 78 K and mechanical properties similar to those of bare LAO resonators. These results open new possibilities toward the development of advanced transducers, such as bolometers or magnetic field detectors, as well as experiments in solid state physics, material science, and quantum opto-mechanics.

1. Introduction

A distinct feature of many transition metal oxides is their compatible crystal lattice and the consequent opportunity to fabricate epitaxial heterostructures showing emergent properties.[1] Paradigmatic realizations of this capability are conductive interfaces hosting superconducting quasi-2D electron gas,[2–4] which can be further manipulated to integrate spin-polarization, ferro-electricity and magnetism.[5,6] Growth of crystalline complex oxides is also possible on pre-patterned suspended oxide thin films, where ex situ etero-epitaxial growth has been demonstrated.[7,8] These full-oxide suspended devices can be characterized by mechanical methods to measure their static displacement or eigenfrequencies, which are related to the mechanical properties of their constituent materials,[9–11] toward the development of new functional micro-electro-mechanical devices.[12,13]

Mechanical resonators are among the most sensitive transducers and are employed in a variety of fields, from biomolecules detection to quantum information processing. A critical parameter of mechanical resonators is their quality factor (*Q*-factor), which is directly related to their capability to sense variations of physical quantities such as mass or tension.[14] *Q*-factor can be enhanced by lowering the relative energy loss per cycle towards the environment at the clamping points. This is possible by increasing the tension of the structures,[15–17] or by realizing specific device geometries that confine the mechanical modes within the resonator.[18–20] Designing complex oxide heterostructures by controlled growth allows for precise stress engineering,[21–24]

N. Manca, A. E. Plaza, L. Cichetto Jr., E. Bellingeri, F. Bisio, D. Marré, L. Pellegrino
CNR-SPIN
C.so F. M. Perrone, 24, Genova 16152, Italy
E-mail: nicola.manca@spin.cnr.it

The ORCID identification number(s) for the author(s) of this article can be found under https://doi.org/10.1002/adfm.202403155

DOI: 10.1002/adfm.202403155

A. Kalaboukhov, E. Wahlberg, F. Lombardi
Department of Microtechnology and Nanoscience – MC2
Chalmers University of Technology
Gothenburg SE 412 96, Sweden

E. Wahlberg
RISE Research Institutes of Sweden
Box 857, Borås SE-50115, Sweden

D. Marré
Dipartimento di Fisica
Università degli Studi di Genova
Genova 16146, Italy

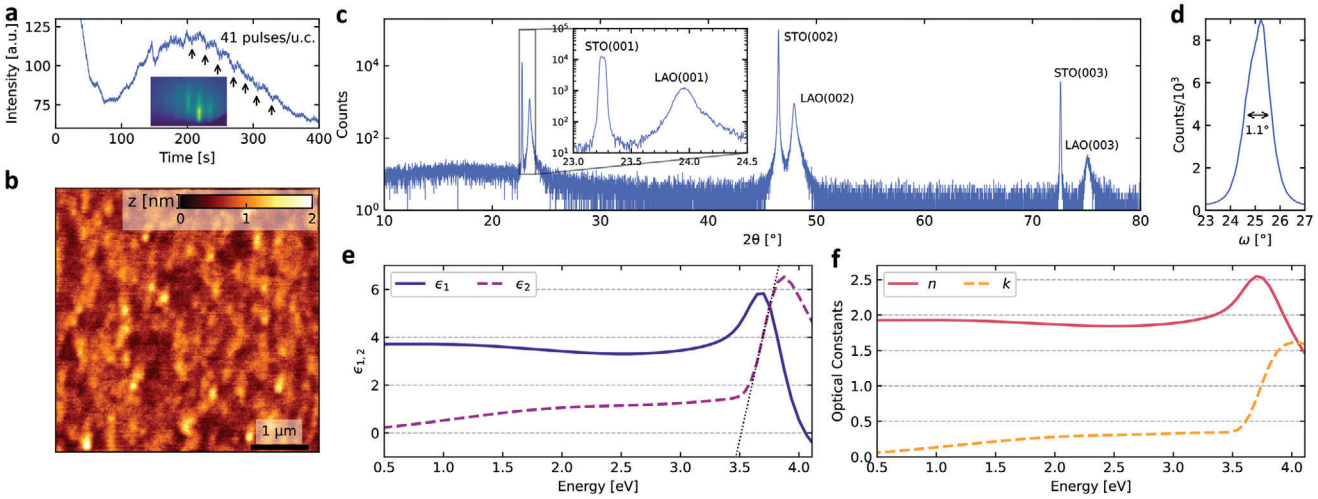

Figure 1. Characterization of $LaAlO_3$ thin films grown on $SrTiO_3$(001). a) Time evolution of the reflection high-energy electron diffraction (RHEED) intensity during the thin film growth. The inset shows the RHEED diffraction pattern at the end of the deposition. b) AFM topography image of the LAO surface. c) X-rays θ–2θ diffraction measurement of the LAO thin film. The inset shows a magnification of the STO and LAO (001) peaks. d) ω-scan (rocking curve) of the LAO(002) peak. e) Coefficients of the complex dielectric response of the LAO thin films and f) corresponding optical constants. An optical bandgap of 3.4 eV is estimated from the intersection at ϵ=0 of the tangent to the onset of the ϵ_2 peak (black dotted line).

making these materials suitable to realize tensile-stressed mechanical resonators with relatively high Q-factor.[25] Thin films of LAO on STO are a good choice for this purpose as they have a lattice mismatch of up to 3%, which leads to a large built-in tensile strain that, during the growth, gets partially relaxed.[26] Moreover, as LAO is a common substrate material for growing many oxides, suspended structures made of LAO are ideal candidates as templates for the realization of functional sensors or actuators.

In this work, we discuss the realization of a device consisting of a high-T_c superconductor grown on top of a high Q-factor oxide mechanical resonator made of a single-crystal suspended LAO micro-bridge. LAO bridges are fabricated from thin films deposited on top of a $SrTiO_3$(001) substrate. Structural and optical properties of pristine LAO films are investigated by X-ray diffraction and spectroscopic ellipsometry. Mechanical characterization of LAO micro-bridges, such as eigenfrequency and Q-factor length dependence, provides the in-plane stress and the intrinsic Q value of the material. We discuss the characteristics of YBCO grown on top of LAO micro-bridges by comparing their crystalline quality and transport properties with those of films grown on a STO(001) substrate. We also characterize the YBCO/LAO resonators at room temperature, in view of the realization of superconducting MEMS.

2. Results and Discussion

$LaAlO_3$ films were deposited by pulsed laser deposition (PLD) on $SrTiO_3$(001) single crystals, as detailed in the Experimental Section. The quality and deposition rate of the LAO film were monitored during the growth by reflection high-energy electron diffraction (RHEED). The time evolution of RHEED intensity is reported in **Figure** 1a and shows oscillations, corresponding to a growth rate of 41 pulses per unit cell, on top of a slow-varying non-monotonic background. Such time evolution has already been observed during the growth of low-stress LAO thin films.[26] The RHEED diffraction pattern at the end of the deposition (inset panel) shows striped features and absence of peaks related to 3D diffraction, as expected from thin films with low roughness. The LAO surface was inspected by atomic force microscopy and is reported in Figure 1b. It has a flat topography with a RMS roughness below 0.3 nm over a 5 × 5 µm^2 area.

Here, we focus on 100 nm thick LAO films because previous studies on other complex oxides MEMS showed that a good fabrication yield requires a film thickness of several tens of nanometers.[10–12,25,27] However, for thickness values above 25 nm the large epitaxial strain in LAO due to the STO substrate relaxes with the formation of cracks across the full height of the deposited films and may result in its delamination from the substrate.[26] Consequently, to obtain LAO films of about 100 nm and resistant to the fabrication of suspended structures we need to lower the built-in strain of the material due to the epitaxial growth. To do so, the simplest approach is to control the growth parameters, in particular the substrate temperature and the oxygen pressure, to promote the formation of defects that can relax the epitaxial strain during the growth, such as oxygen vacancies or dislocations. The resulting films allow to obtain a good fabrication yield of the suspended structures.

Since a certain amount of defects in our LAO films is both expected and desirable, it is relevant to understand their impact on the properties of the deposited material. We characterized the deposited LAO films by combining X-ray diffraction measurements (XRD) and spectroscopic ellipsometry measurements. XRD data reported in Figure 1c were acquired in Bragg-Brentano configuration and show (00l) peaks without spurious phases. The inset panel is a close-up around the (001) peaks of the STO substrate and the LAO film. LAO is tensile strained due to the epitaxial mismatch with STO, with a c-axis of 3.81 Å. Considering the film thickness of 100 nm, the diffraction peak is quite broad, suggesting a low crystal quality. This is also confirmed by the ω-scan (rocking curve) reported in Figure 1d with a full width at half

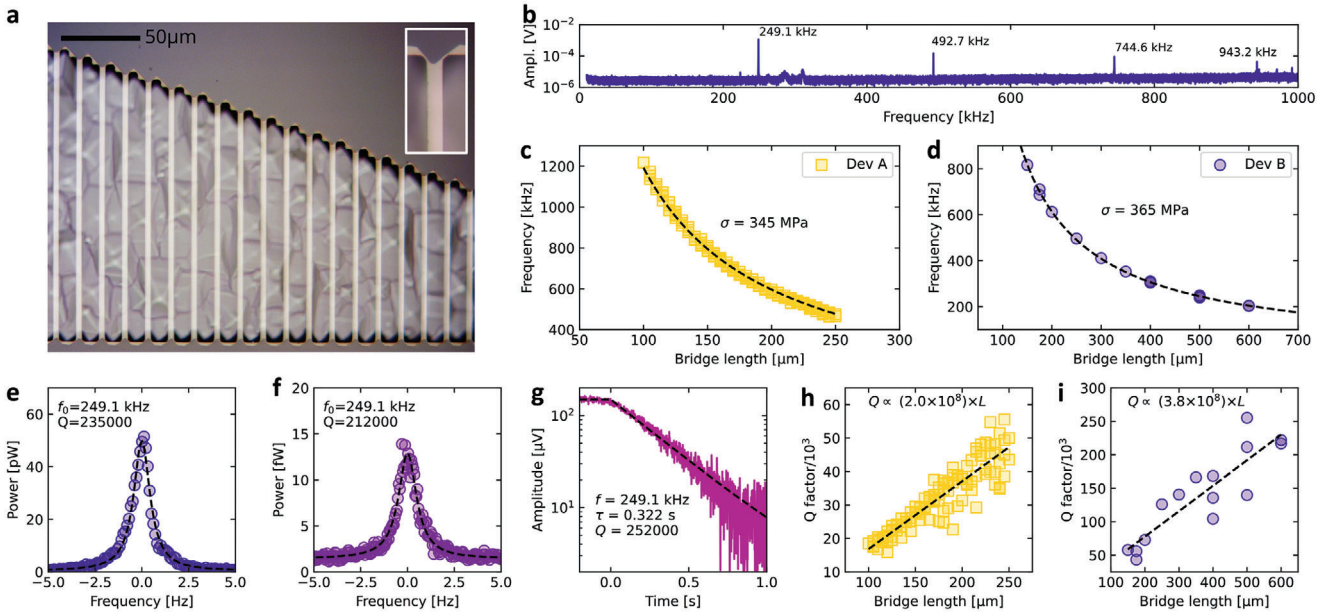

Figure 2. Mechanical characterization of $LaAlO_3$ micro-bridge resonators. a) Optical micrograph of a harp array of LAO bridges. The inset shows a magnification of the clamping region. b) Mechanical spectrum of a 500 μm-long bridge with the first four flexural modes marked with their frequency value. c, d) Length dependence of the eigenfrequency of the first flexural mode for two samples having bridges of different lengths. The black dashed line is the best fit using Equation (1) providing the stress (σ). More than 100 bridges were measured for "Dev A" and 15 for "Dev B". e) Resonance peak under piezoelectric excitation, f) thermomechanical noise spectrum and (g) amplitude decay corresponding to the first flexural mode of the bridge in (a). Units are referred to the electrical signal measured from the detector. h) Length dependence of the Q-factor of the first flexural mode for "Dev A" and (i) "Dev B". The black dashed lines are linear fit.

maximum of 1.1°, a relatively large value that signals the presence of crystallographic defects.

Crystal defects also affect the optical response of LAO, which in bulk form is a transparent insulator with a bandgap of 5.6 eV.[28] We thus checked a possible degradation of LAO optical properties by spectroscopic ellipsometry. Real (ϵ_1) and imaginary (ϵ_2) components of the dielectric response are reported in Figure 1d, while the corresponding optical constants n and k are reported in and Figure 1e. The bandgap of our LAO thin films is 3.5 eV, as obtained from the intersection at zero of the tangent to the maximal slope of ϵ_2 (black dashed line). Its value is lower than the bulk one, but in good agreement with optical transmittance measurements performed on LAO/STO heterostructures under various growth conditions.[29] The presence of defects is particularly visible in the low-energy region, below the bandgap, where ϵ_2 shows broadband absorption due to in-gap states. Despite such small absorption, no significant heating effect during the following mechanical measurements of suspended LAO bridges were observed. Understanding of the interplay between broadband optical absorption and stress relaxation upon different growth conditions is of interest for the design of micro-mechanical devices based on LAO or other complex oxides.

2.1. $LaAlO_3$ Mechanical Resonators

Suspended micro-bridge structures were fabricated by UV lithography and Ar-ion dry etching of the LAO films followed by selective wet etching of the STO substrate in HF bath. Details of the fabrication process are discussed in the Experimental Section and based on previously reported processes for complex oxides micro-resonators.[11,25,27] An example of the fabricated devices is reported in **Figure 2a**, where suspended regions are light and clamped ones are dark. The inset shows a magnification of the clamping region of a bridge. The faceting of the crystal that can be seen in the under-etched regions is determined by the etching anisotropy of the STO substrate in HF.[30] We fabricated two sets of LAO samples, "Dev A" has many short bridges to obtain a robust statistics on the fabrication yeld and mechanical properties, while "Dev B" has very long bridges to explore the limits of the current fabrication protocol. In the first case the micro-bridges length spans from 100 to 250 μm with steps of 5 μm and in the second it spans from 150 to 1000 μm, while the width is always 4 μm.

The mechanical spectra of LAO resonators was measured in the optical lever detection scheme, and mechanical excitation was provided by a piezoelectric element, as detailed in the Experimental Section. Figure 2b shows the mechanical spectrum of a LAO bridge resonator having length 500 μm. The first four flexural modes are marked with their frequency value and are evenly spaced, as expected for a bridge under high tensile stress. In such condition, a bridge resonator is in the string limit and the frequency of the n^{th} flexural modes is given by its density (ρ), its length (L), and the tensile stress (σ):[31]

$$f_n = \frac{n}{2L}\sqrt{\frac{\sigma}{\rho}} \tag{1}$$

The in-plane stress of LAO is obtained from the length dependence of the resonance frequency of the first flexural mode (f_1) in

Figure 2a,b. The experimental data-points are reported together with their fit with Equation (1) (dashed line), showing good agreement. Both the samples show an in-plane tensile stress in the 350 MPa range, a relatively high value that confirms the high stress condition of the LAO film expected from Figure 2b. Considering the difference in lattice constants of STO and LAO (3.90 and 3.79 Å),[32] and the bulk Young modulus for LAO of 170 GPa,[33,34] we estimate the upper limit for stress to be about 5 GPa. This is one order of magnitude higher than what we measured. This lower value is consistent with the formation of defects during the growth, that allows to reduce the stress in order to obtain higher fabrication yield of the suspended structures.

The measurement of the *Q*-factor is a critical aspect to evaluate the performance of a mechanical resonator. In Figure 2e–g we show different evaluation methods of the *Q*-factor of the first flexural mode of the same 500 µm bridge shown in Figure 2a. Reported values are all consistently above 200k. Figure 2e is the resonance power spectrum measured upon piezoelectric excitation and the dashed line is the fit of a Lorentzian function. Figure 2f is the thermo-mechanical noise spectrum in the same frequency region fitted by the thermal noise function.[35] Figure 2g shows the time-dependence of the oscillation amplitude after turning off the piezoelectric excitation ($t = 0$). The time constant of the resonator ringdown (τ) is obtained by fitting an exponential decay function and provides the *Q*-factor ($Q = \pi \tau f_1$).[31]

In tension-dominated mechanical resonators, the stress increases the mechanical *Q*-factor through the dissipation–dilution mechanism,[17,36] which is quantitatively represented by the factor *D*:

$$Q = Q_{\text{int}} \cdot D \tag{2}$$

where Q_{int} is the intrinsic *Q*-factor, a relevant parameter to evaluate the performances of a material for MEMS applications. For a uniform rectangular beam having high aspect ratio, as our LAO bridges ($h/L < 10^{-3}$), if dissipation–dilution is the dominant mechanism determining the *Q*-factor, the latter is proportional to *L*:

$$Q = Q_{\text{int}} \frac{\sqrt{3}}{h} \sqrt{\frac{\sigma}{E}} L \tag{3}$$

where *E* is the Young's modulus and *h* is the thickness.

In Figure 2h,i, we plot the length dependence of the *Q*-factor for the same set of resonators reported in Figure 2c,d, respectively. Despite the spread of the data, which is likely due to the residues on the samples due to the fabrication process still under optimization, the number of measured resonators allows us to identify a linear trend. A linear fit (black line) gives a slope of about $2{\cdot}10^8$ m^{-1} for "Dev A" and $3.8{\times}\,10^8$ m^{-1} for "Dev B", which are rather compatible with each other, considering the dispersion of the data-points. By inverting Equation (3), it is then possible to obtain Q_{int}. Previous reports indicate that the Young's modulus of bulk LAO along the (001) is about 170 GPa.[33,34] However, in 100 nm-thick crystalline films of other oxides compounds, such as $SrTiO_3$ and $EuTiO_3$, a halving of the Young's modulus with respect to the bulk values has been observed,[11,37] which increases the uncertainty over the expected Young's modulus of our devices. The stress of $\sigma \approx$350 MPa corresponds thus to an in-plane strain in the 0.2–0.4 % range, which is in good agreement with previous measurements performed on tensile-strained WO_3 and $(La,Sr)MnO_3$ single crystal micro-bridge resonators.[25,27] The resulting Q_{int} is in between 200 and 500, which is about ten times lower than what recently measured in 100 nm-thick Si_3N_4 resonators having the same length scale.[38] This difference suggests that the relatively high values of mechanical *Q*-factor measured on our LAO resonators could be further enhanced by optimizing material quality and, in case, the fabrication protocol. Better evaluation of Q_{int} can be achieved by direct measurements of the Young's modulus of these thin structures by in situ techniques, such as multi-modal analysis of the bridges' resonance frequencies or AFM force-distance measurements.[37,39]

2.2. YBCO/LAO Micro-Bridges

To demonstrate the potential of LAO suspended structures as templates for ex situ hetero-epitaxial growth of complex oxides thin films, we selected YBCO, a high-T_c superconductor whose critical temperature is strongly affected by its crystal quality and strain.[40] **Figure 3**a,b shows the XRD θ–2θ scans of two 100 nm YBCO films deposited on a single-crystal STO(001) substrate (YBCO/STO) and on LAO after the release of the bridges from the STO substrate (YBCO/LAO/STO). We compare in Figure 3c the (005) peak of the YBCO deposited the STO substrate and on the patterned LAO film. They have an almost identical shape, but the one belonging to the YBCO/LAO/STO shows a +0.09 ° shift, corresponding to a -0.19 % variation in the out-of-plane direction. The YBCO *c*-axis is thus 11.68 Å for the film deposited on the STO substrate, identical to its bulk value, while 11.66 Å for the film deposited on the patterned LAO. We found a more marked difference between the two cases when comparing their rocking curves. ω-scans measurements of the YBCO(005) peaks are reported in Figure 3d, where we also show their full width at half maximum (FWHM), which is an indication of crystalline disorder. A larger value is found for the YBCO/LAO/STO case, signalling lower crystal quality. This is expected, since the growth on STO(001) can be considered an ideal case, while it is relevant to note that the peak width of YBCO on patterned LAO is much lower than the one of the underlying LAO film, which is reported in Figure 1d. Although the diffraction pattern of YBCO on LAO indicates a high crystal quality, showing no spurious phases and an almost identical amplitude of the peaks with respect to the film grown on top of the STO substrate, we can not obtain information about the film deposited on the suspended regions as their volume is negligible with respect to the one of the pad regions.

To directly probe the characteristics of the YBCO film on suspended LAO, we thus performed four-probe electrical transport measurements across a micro-bridge. The temperature dependence of the electrical resistance was measured from 300 K down to 70 K and is reported in **Figure 4** (orange line). The measured bridge has a width of 4 µm and a length of 50 µm and its optical micrograph is included as inset of the same figure panel. The electrical connections were realized by ultrasonic bonding wires on the 200×200 µm^2 pads located at the two ends of a bridge. The YBCO film is found to be superconducting even across the narrow freestanding membrane. The onset of the superconducting transition is at $T_{c,\,on} = 90$ K, reaching zero resistance at about $T_{c,\,0}$

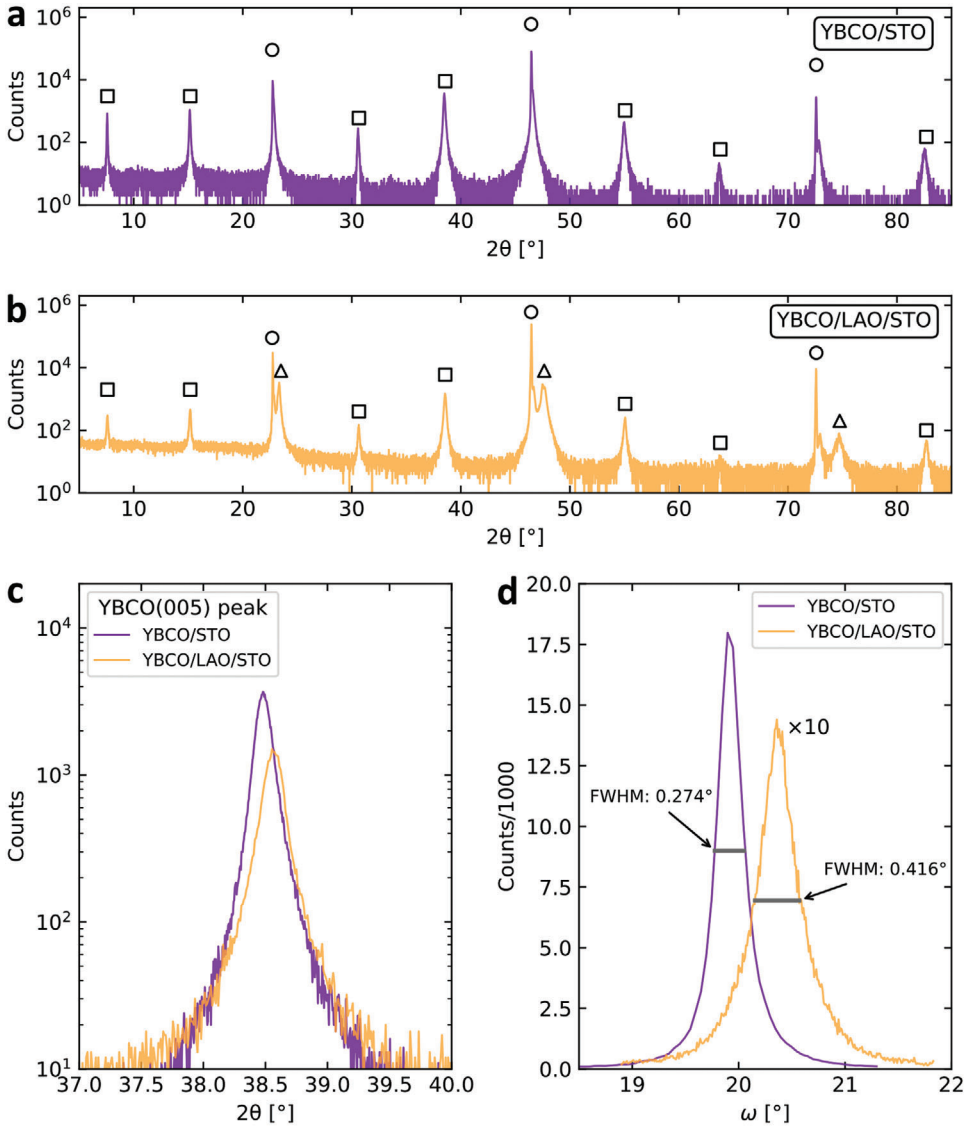

Figure 3. XRD analysis of a 100 nm-thick YBCO film grown on STO(001) substrate (YBCO/STO) and on patterned LAO film after the release of the bridges (YBCO/LAO/STO). a, b) θ–2θ scans of the heterostructures where markers identify the material associated to each (00*l*) peak: STO (◯), LAO (△), and YBCO (□). YBCO(003/6/9) peaks are too close to the STO ones and were not marked. c) Comparison of the (005) diffraction peaks and d) ω-scans of the two cases. In (d) the YBCO/LAO/STO peak is magnified for easier comparison.

= 78 K. The transition on YBCO/LAO/STO is about 10 K, broader than on YBCO/STO (purple line) where it is less than 2 K. This broadening may be caused by various factors, such as crystalline quality, oxygen non-stoichiometry, non-homogeneous strain profiles, or temperature gradients along the suspended LAO bridge. We note that a long post annealing in oxygen atmosphere did not change the superconducting properties and that the XRD data indicate that the *c*-axis lattice parameter of the YBCO/LAO/STO film corresponds to the optimally doped YBCO.[41] In order to elucidate the exact origin of such broadening, detailed measurements of superconducting properties of YBCO films as a function of bridge length and width, as well as a function of deposition parameters are required.

In order to assess the influence of the growth of YBCO on the characteristics of LAO resonators, we measured the mechanical properties at room temperature of about ten YBCO/LAO microbridges having length from 175 µm to 700 µm, to be compared with those of bare LAO resonators reported in Figure 2. **Figure 5**a shows the resonance frequency of the first flexural mode as a function of the bridge length. The stress is obtained by fitting Equation (1) (black dashed line) and is about 180 MPa. This value is one half of the one obtained for bare LAO bridges, indicating that YBCO growth involved some strain relaxation, although not critical if considering the thickness of the YBCO (150 nm). The mechanical *Q*-factor of these bridges was evaluated by ring-down measurements and reported in Figure 5b. The longest one reaches *Q*-factor of about 180k, with a relaxation time constant longer than 500 ms, as reported in Figure 5c. We note that, despite the higher thickness and lower stress, the slope of the *Q* versus *L* relationship is comparable to those measured for bare

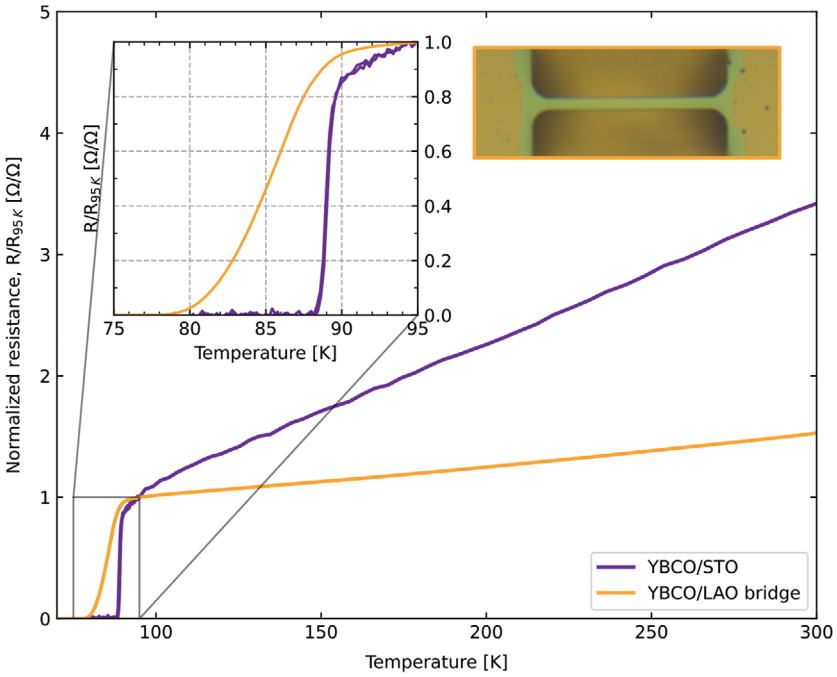

Figure 4. Temperature dependence of the normalized electrical resistance of YBCO deposited on a STO substrate (purple) and a LAO micro-bridge (orange) as those shown in the optical micrograph. The close-up inset shows the resistance evolution around the superconducting transition temperature.

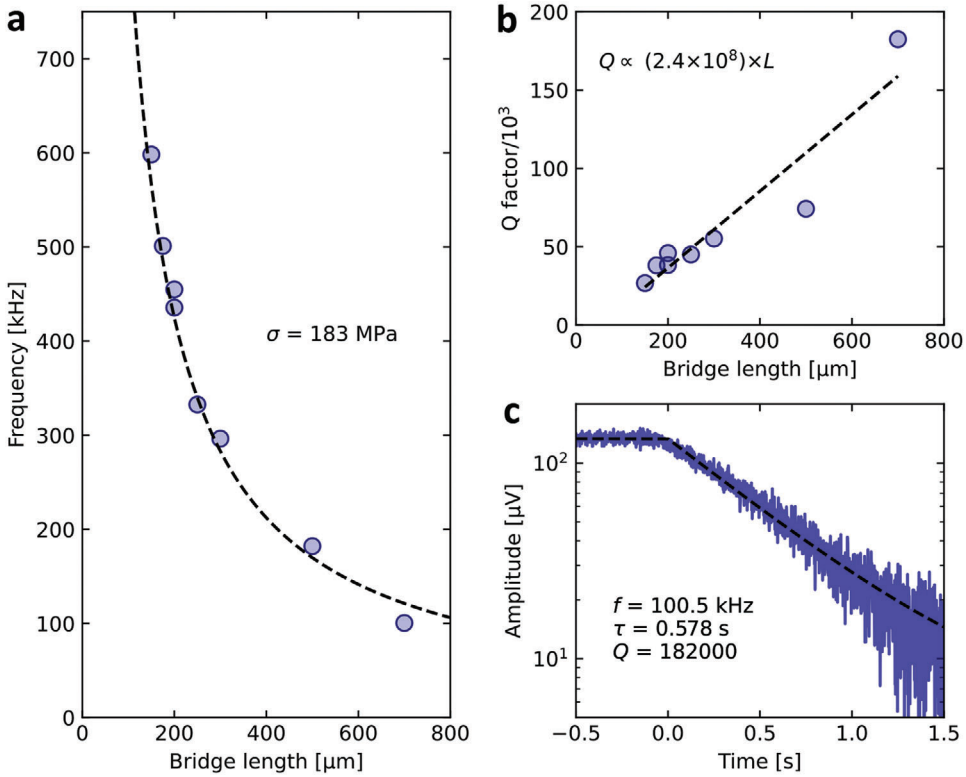

Figure 5. Mechanical properties of YBCO/LAO resonators at room temperature. a) Frequency of the first flexural mode as a function of the bridge length. By fitting Equation (1) (black dashed line), we obtain the tensile stress, σ. b) Quality factor as a function of the bridge length. The slope of the linear fit (black dashed line) is comparable to that of bare LAO bridges. c) Ringdown measurement of a 700 μm-long bridge showing Q-factor above 180k.

LAO. This suggests that intrinsic Q_{int} could be even higher than that of LAO. This effect is likely due to thickness dependence of Q_{int}, as observed in Si devices, and related to the reduction of surface losses with respect to volume ones.[38] These results are very promising for studying the fundamental properties of YBCO and for the fabrication of sensors based on suspended YBCO structures, such as kinetic inductance bolometers, magnetic field sensors, or superconducting opto-mechanical resonators.[42,43]

3. Conclusion

In conclusion, we demonstrated the fabrication of single crystal LAO suspended bridges as templates for ex situ growth of functional complex oxides, choosing the high-T_c superconductor YBCO as functional layer grown ex situ. Mechanical characterization of bare LAO resonators provided an in-plane stress of about 350 MPa, mechanical *Q*-factors as high as 200k, and an intrinsic *Q*-factor in the 200–500 range, which is about one order of magnitude lower than what reported for Si compounds. More experiments are required to clarify the intrinsic limits of this material, and other similar oxides, in terms of mechanical losses, and if they can be improved by controlling the growth conditions and the fabrication processes. Single crystal YBCO thin films deposited on top of LAO bridges show high crystal quality and superconducting behavior. Although further optimization process may be required to reach the sharp transition observed in optimally-doped film grown on STO(001) substrates, zero-resistance state in suspended bridges is reached above the critical threshold of liquid nitrogen temperature. Mechanical properties of suspended YBCO/LAO bridges at room temperature are comparable to those of bare LAO resonators, showing lower stress but similar *Q*-factor values. Potential applications of the presented device include bolometers, magnetometers, or even opto-mechanical experiments related to fundamental studies of the superconducting transition, in particular in its mixed state.

4. Experimental Section

Growth of $LaAlO_3$ Thin Films: LAO films were deposited by pulsed laser deposition on top of not-terminated $SrTiO_3$ (001) single crystal substrates from a 10× 10 ×1 mm^3 single crystal LAO target. The growth temperature was 900 °C, the background oxygen pressure was $1{\cdot}10^{-4}$ mbar, the laser fluency was 2 J cm^{-2}, the laser repetition rate was 2 Hz, and the target-substrate distance was about 3.5 cm. LAO growth rate was of about 70 nm h^{-1}.

Growth of $YBa_2Cu_2O_7$ Thin Films: YBCO thin films were deposited by pulsed laser deposition. The growth temperature was 800 °C, the background oxygen pressure was 0.7 mbar, the laser fluency was 1.25 J cm^{-2}, and the target-substrate distance was 55 mm. In order to prevent damage of the bridges due to differential thermal expansion, the samples were heated and cooled at slow rate of 5 degrees per minute.

Fabrication of the Suspended LAO Bridges: Suspended microstructures were fabricated by UV lithography. SPR-220-4.5 photo-resist was deposited by drop-casting and spin-coated at 6000 RPM for 45 s and then baked at 120 °C for 135 s. LAO etching was performed by Ar Ion milling in a system equipped with a water-cooled sample holder. Etching time was 45 min, with Ar ions energy of 500 eV and current density of 0.2 mA m^{-2}. Photo-resist was removed in an acetone ultrasonic bath at room temperature, followed by an ethanol bath. The STO substrate was selectively etched by soaking the samples in a 5 % HF aqueous solution kept at 35 °C in bain-marie for 30 min. During the bath, the samples were kept suspended above a magnetic stirrer rotating at 200 RPM. They were then transferred in a deionized water bath, followed by two different baths of pure ethanol to remove the presence of water. Finally, they were dried in a CO_2 critical point dryer system.

Mechanical Resonance Measurements: Mechanical spectral response of the resonators was measured at 25 °C in a custom setup featuring active temperature control and base pressure of $2{\cdot}10^{-5}$ mbar. Device motion was probed by optical lever detection scheme. Mechanical excitation was provided by a AC-biased piezoelectric element glued by ceramic epoxy nearby the device.

Statistical Analysis: All the results reported in this work were obtained by analyzing the raw data acquired from the instruments. Data analysis was performed by using a Python script which was included in the data repository (see "Data Availability Statement").

Acknowledgements

N.M. thanks Giordano Mattoni for the useful comments on the draft article. This work was carried out under the OXiNEMS project (www.oxinems.eu). This project has received funding from the European Union's Horizon 2020 research and innovation programme under Grant Agreement No. 828784. The authors acknowledge financial support from the Università di Genova through the "Fondi di Ricerca di Ateneo" (FRA). The authors also acknowledge support from the Swedish infrastructure for micro- and nano-fabrication - MyFab. [Correction added on August 6, 2024, after first online publication: Typographical errors have been updated in this version.]

Conflict of Interest

The authors declare no conflict of interest.

Data Availability Statement

The data that support the findings of this study are openly available in Zenodo at https://doi.org/10.5281/zenodo.10521695, reference number 10521695.

Keywords

$LaAlO_3$, Oxide Nanomechanics, Oxide Resonators, Superconducting MEMS, YBCO

Received: February 21, 2024
Revised: June 13, 2024
Published online: July 17, 2024

[1] R. Ramesh, D. G. Schlom, *Nat. Rev. Mater* **2019**, *4*, 257.
[2] P. Zubko, S. Gariglio, M. Gabay, P. Ghosez, J.-M. Triscone, *Annu. Rev. Condens. Matter Phys.* **2011**, *2*, 141.
[3] Y.-Y. Pai, H. Lee, J.-W. Lee, A. Annadi, G. Cheng, S. Lu, M. Tomczyk, M. Huang, C.-B. Eom, P. Irvin, J. Levy, *Phys. Rev. Lett.* **2018**, *120*, 147001.
[4] D. V. Christensen, F. Trier, W. Niu, Y. Gan, Y. Zhang, T. S. Jespersen, Y. Chen, N. Pryds, *Adv. Mater. Interfaces* **2019**, *6*, 1900772.
[5] D. Stornaiuolo, C. Cantoni, G. M. De Luca, R. Di Capua, E. Di. Gennaro, G. Ghiringhelli, B. Jouault, D. Marrè, D. Massarotti, F. Miletto Granozio, I. Pallecchi, C. Piamonteze, S. Rusponi, F. Tafuri, M. Salluzzo, *Nat. Mater* **2016**, *15*, 278.

[6] J. Bréhin, Y. Chen, M. D'Antuono, S. Varotto, D. Stornaiuolo, C. Piamonteze, J. Varignon, M. Salluzzo, M. Bibes, *Nat. Phys.* **2023**, *19*, 823.
[7] M. Biasotti, L. Pellegrino, E. Bellingeri, N. Manca, A. S. Siri, D. Marrè, *Appl. Phys. Lett.* **2010**, *97*, 223503.
[8] L. Pellegrino, N. Manca, T. Kanki, H. Tanaka, M. Biasotti, E. Bellingeri, A. S. Siri, D. Marré, *Adv. Mater.* **2012**, *24*, 2929.
[9] D. Davidovikj, D. J. Groenendijk, A. M. R. V. L. Monteiro, A. Dijkhoff, D. Afanasiev, M. Šiškins, M. Lee, Y. Huang, E. van Heumen, H. S. J. van der Zant, A. D. Caviglia, P. G. Steeneken, *Commun. Phys.* **2020**, *3*, 163.
[10] N. Manca, T. Kanki, F. Endo, E. Ragucci, L. Pellegrino, D. Marré, *ACS Appl. Electron. Mater.* **2021**, *3*, 211.
[11] N. Manca, G. Tarsi, A. Kalaboukhov, F. Bisio, F. Caglieris, F. Lombardi, D. Marré, L. Pellegrino, *APL Mater.* **2023**, *11*, 101107.
[12] N. Manca, T. Kanki, F. Endo, D. Marré, L. Pellegrino, *Nano Lett.* **2020**, *20*, 7251.
[13] M. Lee, J. R. Renshof, K. J. van Zeggeren, M. J. A. Houmes, E. Lesne, M. Šiškins, T. C. van Thiel, R. H. Guis, M. R. van Blankenstein, G. J. Verbiest, A. D. Caviglia, H. S. J. van der Zant, P. G. Steeneken, *Adv. Mater.* **2022**, *34*, 2204630.
[14] S. S. Verbridge, J. M. Parpia, R. B. Reichenbach, L. M. Bellan, H. G. Craighead, *J. Appl. Phys.* **2006**, *99*, 124304.
[15] Y. Tsaturyan, A. Barg, E. S. Polzik, A. Schliesser, *Nat. Nanotech.* **2017**, *12*, 776.
[16] S. A. Fedorov, N. J. Engelsen, A. H. Ghadimi, M. J. Bereyhi, R. Schilling, D. J. Wilson, T. J. Kippenberg, *Phys. Rev. B* **2019**, *99*, 054107.
[17] L. Sementilli, E. Romero, W. P. Bowen, *Adv. Funct. Mater.* **2022**, *32*, 2105247.
[18] D. Shin, A. Cupertino, M. H. J. de Jong, P. G. Steeneken, M. A. Bessa, R. A. Norte, *Adv. Mater.* **2022**, *34*, 2106248.
[19] M. J. Bereyhi, A. Beccari, R. Groth, S. A. Fedorov, A. Arabmoheghi, T. J. Kippenberg, N. J. Engelsen, *Nat Commun* **2022**, *13*, 3097.
[20] Z. Li, M. Xu, R. A. Norte, A. M. Aragón, F. van Keulen, F. Alijani, P. G. Steeneken, *Appl. Phys. Lett.* **2023**, *122*, 013501.
[21] J. Zhang, H. Tanaka, T. Kanki, J.-H. Choi, T. Kawai, *Phys. Rev. B* **2001**, *64*, 184404.
[22] J. L. MacManus-Driscoll, P. Zerrer, H. Wang, H. Yang, J. Yoon, A. Fouchet, R. Yu, M. G. Blamire, Q. Jia, *Nat. Mater.* **2008**, *7*, 314.
[23] J. Cao, J. Wu, *Mater. Sci. Eng.: R: Rep.* **2011**, *71*, 35.
[24] G. Mattoni, N. Manca, M. Hadjimichael, P. Zubko, A. J. H. Van Der Torren, C. Yin, S. Catalano, M. Gibert, F. Maccherozzi, Y. Liu, S. S. Dhesi, A. D. Caviglia, *Phys. Rev. Mater.* **2018**, *2*, 085002.
[25] N. Manca, F. Remaggi, A. E. Plaza, L. Varbaro, C. Bernini, L. Pellegrino, D. Marré, *Small* **2022**, *18*, 2202768.
[26] A. Sambri, M. Scuderi, A. Guarino, E. D. Gennaro, R. Erlandsen, R. T. Dahm, A. V. Bjørlig, D. V. Christensen, R. D. Capua, B. D. Ventura, U. S. D. Uccio, S. Mirabella, G. Nicotra, C. Spinella, T. S. Jespersen, F. M. Granozio, *Adv. Funct. Mater.* **2020**, *30*, 1909964.
[27] N. Manca, G. Mattoni, M. Pelassa, W. J. Venstra, H. S. J. van der Zant, A. D. Caviglia, *ACS Appl. Mater. Interfaces* **2019**, *11*, 44438.
[28] P. W. Peacock, J. Robertson, *J. Appl. Phys.* **2002**, *92*, 4712.
[29] W. S. Choi, C. M. Rouleau, S. S. A. Seo, Z. Luo, H. Zhou, T. T. Fister, J. A. Eastman, P. H. Fuoss, D. D. Fong, J. Z. Tischler, G. Eres, M. F. Chisholm, H. N. Lee, *Adv. Mater.* **2012**, *24*, 6423.
[30] A. E. Plaza, N. Manca, C. Bernini, D. Marré, L. Pellegrino, *Appl. Phys. Lett.* **2021**, *119*, 033504.
[31] S. Schmid, L. G. Villanueva, M. L. Roukes, *Fundamentals of Nanomechanical Resonators*, Springer International Publishing, Cham **2016**.
[32] L. John Berchmans, S. Angappan, A. Visuvasam, K. B. Ranjith Kumar, *Mater. Chem. Phys.* **2008**, *109*, 113.
[33] R. J. Harrison, S. A. T. Redfern, A. Buckley, E. K. H. Salje, *J. Appl. Phys.* **2004**, *95*, 1706.
[34] M. A. Carpenter, A. Buckley, P. A. Taylor, T. W. Darling, *J. Phys.: Condens. Matter* **2010**, *22*, 035405.
[35] B. Hauer, C. Doolin, K. Beach, J. Davis, *Ann. Phys.* **2013**, *339*, 181.
[36] N. J. Engelsen, A. Beccari, T. J. Kippenberg, *Nat. Nanotechnol.* **2024**, *19*, 725.
[37] V. Harbola, S. Crossley, S. S. Hong, D. Lu, Y. A. Birkhölzer, Y. Hikita, H. Y. Hwang, *Nano Lett.* **2021**, *21*, 2470.
[38] L. G. Villanueva, S. Schmid, *Phys. Rev. Lett.* **2014**, *113*, 227201.
[39] Y. S. Klaß, J. Doster, M. Bückle, R. Braive, E. M. Weig, *Appl. Phys. Lett.* **2022**, *121*, 083501.
[40] M. Mazini, S. Favre, D. Ariosa, R. Faccio, *Appl. Phys. A* **2022**, *128*, 1111.
[41] P. Benzi, E. Bottizzo, N. Rizzi, *J. Cryst. Growth* **2004**, *269*, 625.
[42] A. Chakrabarty, M. A. Lindeman, B. Bumble, A. W. Kleinsasser, W. A. Holmes, D. Cunnane, *Appl. Phys. Lett.* **2019**, *114*, 132601.
[43] F. Maspero, G. Gatani, S. Cuccurullo, R. Bertacco, in *2021 IEEE 34th Int. Conf. Micro Electro Mech. Syst. MEMS*, IEEE, Gainesville, FL, USA, **2021**, pp. 374–377.